Ambipolar drift of spatially separated electrons and holes

M. Beck,* D. Streb, M. Vitzethum, P. Kiesel, S. Malzer, C. Metzner, and G. H. Döhler
Institut für Technische Physik I, Universität Erlangen–Nürnberg, Erlangen, Germany
(Received 9 January 2001; published 2 August 2001)

We report on the ambipolar transport process of photogenerated, spatially separated charge carriers in the doping layers of a *p-i-n* diode under the influence of lateral electric fields. By including externally applied electric fields into the theory of ambipolar diffusion of spatially separated electrons and holes, we show that the transport of excess carriers can be described as a combined drift and diffusion process. Compared to the well-known ambipolar transport in bulk material, the ambipolar diffusion process is enhanced by several orders of magnitude, whereas the ambipolar drift can be described by the same ambipolar mobility as in bulk material if the electric fields in both doping layers are identical. One major difference of the ambipolar drift of electrons and holes propagating in different layers in comparison to bulk material is the possibility to control the ambipolar mobility dynamically by changing the dark carrier densities by varying the reverse bias applied to the *p-i-n* structure. Most interesting however, is the fact that the ambipolar drift can be controlled by different external fields for electrons and holes. In order to verify the predictions of our theoretical description of the ambipolar transport of spatially separated electrons and holes, we have developed a new pump-and-probe technique that allows for a direct temporally and spatially resolved investigation of the various transport scenarios. The results agree very well with the theoretical simulations.

DOI: 10.1103/PhysRevB.64.085307 PACS number(s): 73.40.−c, 73.43.−f, 73.50.−h

I. INTRODUCTION

The ambipolar diffusion of electrons and holes separated by space charge fields in *p-i-n* diodes or in *n-i-p-i* structures[1] has been of great interest over the last decade. In comparison to a common plasma of electrons and holes, two major differences have been observed. First, due to their separation, the carriers can hardly recombine internally, which results in lifetimes in the range of microseconds to seconds,[2] thus exceeding typical carrier lifetimes in bulk semiconductor material (~ 1 ns) by up to about nine orders of magnitude. Second, because of the reduced Coulomb attraction between carriers of opposite sign due to the separation, the repulsion between carriers of the same sign yields a diffusion process that is enhanced by internally generated lateral electric fields. Although the transport mechanism is more complex if electrons and holes are separated from each other, it can still be described by a single ambipolar diffusion equation.[1] In *p-i-n* diodes[4,5] as well as in *n-i-p-i* superlattices[6] the diffusion coefficient has been shown to exceed the bulk diffusion constant by several orders of magnitude. Both the enhanced diffusion and the enhanced carrier lifetime, resulting from their spatial separation, lead to diffusion lengths that are very much larger than the dimensions of the structures under consideration. This implies that the carrier lifetime can be regarded as infinite compared to the time a carrier spends within the sample, i.e., the carrier lifetime is mainly limited by external recombination at the contacts, not by internal recombination.

Thus, the enhanced ambipolar diffusion is fairly well understood and theory and experiment are in very good agreement.[1,6–9] However, the influence of externally applied lateral electric fields on the transport process of spatially separated carriers has not yet been considered. For a neutral plasma, this process is well known as the ''ambipolar drift.'' In this paper, we will first develop the theory describing the transport under these conditions. Subsequently we will show that the theoretical predictions are in very good agreement with the results of pump-and-probe experiments designed to observe excess carriers in *p-i-n* diodes temporally and spatially resolved.

We solely refer to *p-i-n* diodes here. However, *n-i-p-i* structures can be described within the same framework. Furthermore, we restrict our discussion to the case where the external fields applied to the two doping layers are the same (it should be noted, however, that different external fields can be applied in such systems). This special case simplifies the theory significantly and allows us to define an ambipolar mobility, which is not possible in the case of different fields in the *n* and *p* layers. We show that, in contrast to the enhancement of the diffusion constant, the ambipolar mobility is unaffected by the spatial separation of the carriers.

In the following section we develop the theoretical framework. In the third section the investigated sample and the experimental setup will be described briefly. In Sec. IV we present the results of numerical calculations based on the ambipolar transport model derived in Sec. II and compare these with the results from the experiment described in Sec. III. Finally a conclusion will be given in Sec. V.

II. THEORY

In this section we will show that the transport of photogenerated carriers in separated layers can be described in a similar way as the transport in bulk material, the major difference being the enhanced diffusion coefficient.

A. Bulk semiconductor

To derive the transport equation for separated carriers, we briefly review the simpler case of bulk material. Let the steady-state electron and hole current densities be given by

 ©2001 The American Physical Society

$$\vec{j}_n^0 = e\mu_n n_0 \vec{E}^0 + eD_n \vec{\nabla} n_0,$$
$$\vec{j}_p^0 = e\mu_p p_0 \vec{E}^0 - eD_p \vec{\nabla} p_0, \tag{1}$$

where $\mu_{n,p}$ denote the electron and hole mobilities, $D_{n,p}$ the respective diffusion constants, n_0 and p_0 the steady-state carrier densities, and $\vec{E}^0$ the electric field. If we locally excite additional electron-hole pairs, charges will always be screened by carriers of the opposite charge such that net charges will only occur on a very small scale. Therefore, we assume ambipolarity:

$$\Delta n = n - n_0 = \Delta p = p - p_0 = \rho. \tag{2}$$

Furthermore, the Einstein relations $D_{n,p} = \mu_{n,p}(k_B T/e)$ are assumed to be valid. Since in general, the mobilities of electrons and holes differ, an additional electric field $\Delta\vec{E}^{\text{bulk}}$ will build up until Eq. (2) is fulfilled. The current densities therefore change by the amount

$$\Delta\vec{j}_n = e\mu_n n \Delta\vec{E}^{\text{bulk}} + e\mu_n \rho\vec{E}^0 + k_B T\mu_n \vec{\nabla}\rho,$$
$$\Delta\vec{j}_p = e\mu_p p \Delta\vec{E}^{\text{bulk}} + e\mu_p \rho\vec{E}^0 - k_B T\mu_p \vec{\nabla}\rho. \tag{3}$$

Ambipolarity [Eq. (2)] together with the continuity equations

$$\frac{\partial n}{\partial t} = \frac{1}{e}\vec{\nabla}\cdot\Delta\vec{j}_n + G - R,$$
$$\frac{\partial p}{\partial t} = -\frac{1}{e}\vec{\nabla}\cdot\Delta\vec{j}_p + G - R \tag{4}$$

(G and R denote the deviations of the generation and recombination rates from their respective steady state values) yields

$$0 = \frac{\partial n}{\partial t} - \frac{\partial p}{\partial t} = \vec{\nabla}\cdot\Big[(\mu_n n + \mu_p p)\Delta\vec{E}^{\text{bulk}} + (\mu_n + \mu_p)\rho\vec{E}^0 + \frac{k_B T}{e}(\mu_n - \mu_p)\vec{\nabla}\rho\Big]. \tag{5}$$

Thus, the additional internal electric field amounts to

$$\Delta\vec{E}^{\text{bulk}} = \frac{\text{const}}{\mu_n n + \mu_p p} - \frac{\mu_n + \mu_p}{\mu_n n + \mu_p p}\rho\vec{E}^0 - \frac{\mu_n - \mu_p}{\mu_n n + \mu_p p}\frac{k_B T}{e}\vec{\nabla}\rho. \tag{6}$$

The integration constant depends on the boundary conditions and vanishes in an infinite sample. Inserting $\Delta\vec{E}^{\text{bulk}}$ into Eq. (3), one obtains the well-known continuity equation for ambipolar transport due to the excess carrier density ρ in bulk semiconductors:[3]

$$\frac{\partial\rho}{\partial t} = \frac{1}{e}\vec{\nabla}\cdot\Delta\vec{j}_n + G - R = \vec{\nabla}\Bigg(\underbrace{\frac{\mu_n\mu_p(p-n)}{\mu_n n + \mu_p p}\vec{E}^0}_{\vec{v}^{\text{bulk}}_{\text{drift,ambi}} = \mu^{\text{bulk}}_{\text{ambi}}\vec{E}^0}\rho + \underbrace{\frac{\mu_n\mu_p(p+n)}{\mu_n n + \mu_p p}\frac{k_B T}{e}}_{D^{\text{bulk}}_{\text{ambi}}}\vec{\nabla}\rho\Bigg) + G - R = -\frac{1}{e}\vec{\nabla}\cdot\Delta\vec{j}_p + G - R. \tag{7}$$

B. Spatially separated electrons and holes

Electrons and holes generated by photoexcitation in the intrinsic layer of a p-i-n diode will be separated into the doping layers by the builtin field within a few picoseconds. Since this time is very short compared to the relevant time scale (nano seconds to milliseconds) for the lateral transport, we assume an instantaneous separation of the carriers.

Besides the strongly enhanced recombination lifetime, the spatial separation of electrons and holes has two major effects on the theoretical description of the lateral transport. First, we have to change the three-dimensional vectors into two-dimensional in-plane vectors, carrier densities also become two-dimensional and are only defined within the layers and the unit of the current densities becomes A/m. Second, both the external and the internal fields can differ between the two layers. Therefore, we have to replace $\vec{E}^0$ by $\vec{E}_n^0$ and $\vec{E}_p^0$, and $\Delta\vec{E}^{\text{bulk}}$ by $\Delta\vec{E}_n^{p\text{-}i\text{-}n}$ and $\Delta\vec{E}_p^{p\text{-}i\text{-}n}$, respectively. Eq. (3) then becomes

$$\Delta\vec{j}_n = e\mu_n n \Delta\vec{E}_n^{p\text{-}i\text{-}n} + e\mu_n \rho\vec{E}_n^0 + k_B T\mu_n \vec{\nabla}\rho,$$
$$\Delta\vec{j}_p = e\mu_p p \Delta\vec{E}_p^{p\text{-}i\text{-}n} + e\mu_p \rho\vec{E}_p^0 - k_B T\mu_p \vec{\nabla}\rho. \tag{8}$$

Since the difference between the electric potentials in the two doping layers $\phi_p - \phi_n$ is given by the carrier densities via the capacity density of the diode C_{pn}, we can replace $\Delta\vec{E}_p^{p\text{-}i\text{-}n}$ as follows:

$$\Delta\vec{E}_p^{p\text{-}i\text{-}n} = \Delta\vec{E}_n^{p\text{-}i\text{-}n} - \vec{\nabla}(\phi_p - \phi_n) = \Delta\vec{E}_n^{p\text{-}i\text{-}n} - \frac{\partial(\phi_p - \phi_n)}{\partial\rho}\cdot\vec{\nabla}\rho$$
$$= \Delta\vec{E}_n^{p\text{-}i\text{-}n} - \frac{e}{C_{pn}}\vec{\nabla}\rho. \tag{9}$$

Assuming ambipolarity [Eq. (2)], one obtains

$$
\begin{aligned}
0 &= \frac{\partial n}{\partial t} - \frac{\partial p}{\partial t} \\
&= \frac{1}{e}(\vec{\nabla}\cdot\Delta\vec{j}_n + \vec{\nabla}\cdot\Delta\vec{j}_p) \\
&= \vec{\nabla}\cdot\Big((\mu_n n + \mu_p p)\Delta\vec{E}_n^{p\text{-}i\text{-}n} + (\mu_n\vec{E}_n^0 + \mu_p\vec{E}_p^0)\rho \\
&\quad + \frac{k_B T}{e}(\mu_n - \mu_p)\vec{\nabla}\rho - \mu_p p\frac{e}{C_{pn}}\vec{\nabla}\rho\Big). \qquad (10)
\end{aligned}
$$

Solving for $\Delta\vec{E}_n^{p\text{-}i\text{-}n}$ yields

$$
\Delta\vec{E}_n^{p\text{-}i\text{-}n} = \frac{\text{const}}{\mu_n n + \mu_p p} - \frac{\mu_n\vec{E}_n^0 + \mu_p\vec{E}_p^0}{\mu_n n + \mu_p p}\rho - \frac{\mu_n - \mu_p}{\mu_n n + \mu_p p}\frac{k_B T}{e}\vec{\nabla}\rho + \frac{\mu_p p}{\mu_n n + \mu_p p}\frac{e}{C_{pn}}\vec{\nabla}\rho. \qquad (11)
$$

Again, the integration constant depends on the boundary conditions and vanishes if we assume an infinite sample. Inserting Eq. (11) into Eq. (8), one obtains the continuity equation for the lateral transport of spatially separated excess carriers:

$$
\frac{\partial\rho}{\partial t} = \frac{1}{e}\vec{\nabla}\cdot\Delta\vec{j}_n + G - R = \vec{\nabla}\Bigg[\underbrace{\frac{\mu_n\mu_p(p\vec{E}_n^0 - n\vec{E}_p^0)}{\mu_n n + \mu_p p}}_{\vec{v}_{\text{drift,ambi}}^{\,p\text{-}i\text{-}n}}\rho + \underbrace{\left(\frac{\mu_n\mu_p(p+n)}{\mu_n n + \mu_p p}\frac{k_B T}{e}\right.}_{D_{\text{ambi}}^{\text{bulk}}} + \underbrace{\left.\frac{\mu_n\mu_p np}{\mu_n n + \mu_p p}\frac{e}{C_{pn}}\right)}_{D_{\text{ambi}}^{p\text{-}i\text{-}n}}\vec{\nabla}\rho\Bigg] + G = -\frac{1}{e}\vec{\nabla}\cdot\Delta\vec{j}_p + G - R. \qquad (12)
$$

Comparing Eq. (12) with Eq. (7) we note two important differences. First we observe that there is now, apart from the usual ambipolar bulk contribution to the diffusion current, another term, which originates from the spatial separation of electrons and holes in the *p-i-n* diode and which is also proportional to the gradient of the photoinduced excess charge density. Therefore, this term can be interpreted as an additional contribution to the diffusion current. In fact, the term, $D_{\text{ambi}}^{p\text{-}i\text{-}n}$, is typically by several orders of magnitude larger than the first one, $D_{\text{ambi}}^{\text{bulk}}$, as the voltages $e\,np/(n+p)C_{pn}$ are typically in the range of several volts whereas kT/e is in the mV range. This term is responsible for the ''giant ambipolar diffusion coefficient'' discussed previously.[1,4–9] Second, we see that the drift velocity of the photo-induced excess carrier density, $\vec{v}_{\text{drift,ambi}}$ can no longer be expressed by an ambipolar drift mobility, $\vec{v}_{\text{drift,ambi}} = \mu_{\text{ambi}}\vec{E}_0$ unless $E_p^0 = E_n^0$. In the general case $E_p^0 \neq E_n^0$, the drift velocity still depends on the difference between the hole and electron density, p and n, but now weighted reciprocally with the fields E_n^0 and E_p^0, respectively. Therefore, the sign of the drift velocity can change, depending on whether $E_n^0 >$ or $< (n/p)E_p^0$, although the sign of E_p^0 and E_n^0 may be the same. This implies intriguing consequences for the ambipolar transport. In this paper we will restrict our discussion mostly to the case $E_p^0 = E_n^0$ and only briefly outline a few consequences for the general case $E_p^0 \neq E_n^0$ in Sec. V.

In the following we will also consider only the case of transport in one dimension, chosen to be the x direction. This approximation is strictly valid in a system with translational symmetry along the y direction. If the dimension in the x direction is much larger than the one in the y direction, the carriers will have spread almost equally over the sample's width when $t > L_y^2/D_{\text{ambi}}$. Then, the system can be described with the boundary condition that there is no net current in the y direction, so that the one-dimensional description is also valid. It is worth noting here that there is no surface recombination, since the surface band bending prevents both electrons in n-type material and holes in p-type material to reach the surface. This has previously been verified experimentally.[1] When the excess carrier concentration ρ is small compared to the dark carrier concentrations n_0 and p_0, the ambipolar mobility as well as the ambipolar diffusion coefficient ($D_{\text{ambi}} := D_{\text{ambi}}^{\text{bulk}} + D_{\text{ambi}}^{p\text{-}i\text{-}n}$) are to a good approximation constant. In this ''small-signal case,'' Eq. (12) has the analytical solution

$$
\rho(x,t>0) = \frac{N}{\sqrt{4\pi t D_{\text{ambi}}}}\exp\left(-\frac{(x - v_{\text{drift}}t)^2}{4D_{\text{ambi}}t}\right), \qquad \rho(x,t<0) = 0, \qquad (13)
$$

if the carriers are generated by a spatially and temporally δ-shaped pulse at $x=0$ and $t=0$, provided that no additional boundary conditions are to be taken into account. N specifies the total number of carriers generated per unit length in the y direction. Hence, the small-signal solution is a Gaussian-shaped distribution broadening with the diffusion constant D_{ambi} and drifting with the velocity $v_{\text{drift}} = \mu_{\text{ambi}}^{p\text{-}i\text{-}n}E^{\text{ext}}$.

The dynamics of the diffusion process of photogenerated charge carriers is fairly well understood.[1,7–9] However, Eq. (12) cannot be solved analytically if ρ is not small compared to n_0 or p_0 (''large-signal case'') or if the finite size of the sample has to be considered. Therefore, in order to predict the dynamics of the excess carriers, we have carried out numerical simulations that essentially represent a numerical in-

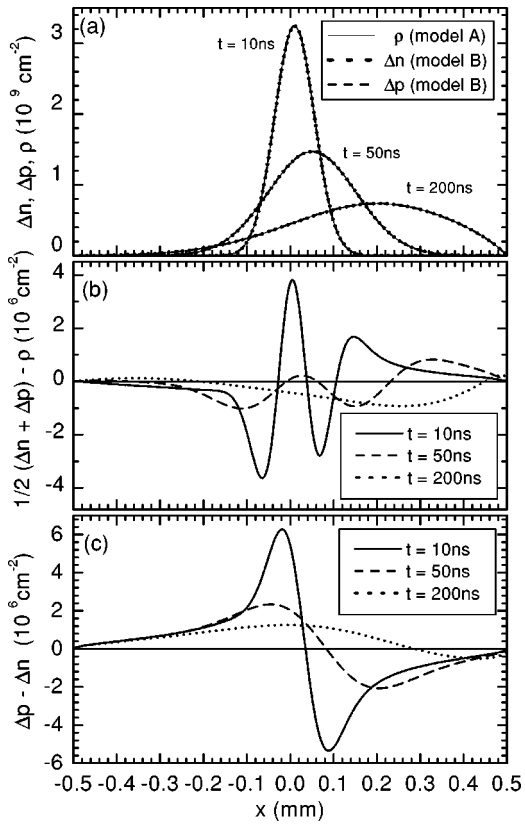

FIG. 1. (a) Excess carrier densities calculated with the assumption $\rho=\Delta n=\Delta p$ (model A) and without this assumption (model B). (b) Comparison between the two numerical models: $(\Delta n+\Delta p)/2-\rho$. (c) Deviations from ambipolarity $\Delta p-\Delta n$; this small deviation allows for ambipolarity by generating lateral electric fields.

tegration of Eq. (12) in a one-dimensional (1D) model system, taking into account realistic boundary conditions given by the contact potentials and including the screening of the external field by the photogenerated carriers (the integration constant neglected in the derivation).

In order to justify the assumptions made in the derivation of Eq. (12), especially the assumption of ambipolarity, i.e., that the space charges within a layer are always screened by an opposite charge in the other layer, we carried out numerical calculations without this assumption and simulated the transport process by solving iteratively Poisson's equation and the continuity equations (4). We restricted the calculations to a model system of two δ-doped layers (two 1D systems interacting with each other), which allows for moderate computing times compared to the more realistic case (one 2D system). Figure 1(a) depicts several snapshots of the calculated distributions of excess electrons Δn and holes Δp (model B) together with the equivalent excess carrier concentrations ρ calculated with the numerically much simpler integration of Eq. (12) (model A). In the example shown, we assumed a model sample with the dark carrier concentrations $n_0=10^{12}$ cm^{-2} and $p_0=4\times10^{12}$ cm^{-2}. The width of the intrinsic layer was assumed to be 100 nm, $L_x=1$ mm, and $U_{\rm lat}=20$ V. The excitation at $L_x/2$ and $t=0$ produced only few carriers compared to the dark carrier concentrations (small-signal case). The deviations between the two models

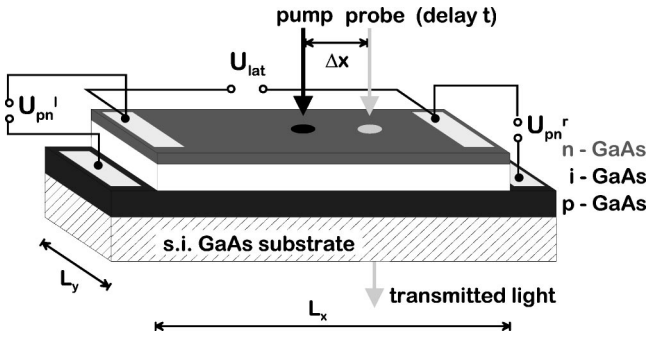

FIG. 2. Schematic view of the sample and the principle of the pump-and-probe experiment.

$(\Delta n+\Delta p)/2-\rho$ are shown in Fig. 1(b), the deviations from ambipolarity $\Delta p-\Delta n$ in Fig. 1(c). In various simulations using a broad spectrum of parameters, we never observed deviations lager than 1%, also in the large-signal case.

III. EXPERIMENT

A. Sample

The sample under investigation is a stripe-shaped gallium arsenide *p-i-n* diode grown by molecular beam epitaxy on a semi-insulating substrate. The layer structure diode consists of a 500 nm thick *p*-doped layer ($n_A=7.5\times10^{16}$ cm^{-3}) deposited on a semi-insulating GaAs substrate, followed by 700 nm intrinsic material and a 320 nm thick *n*-doped layer ($n_D=4.6\times10^{16}$ cm^{-3}) on top. Mesas, as shown schematically in Fig. 2, were defined by photolithography and stepwise etching. The length of the sample ($L_x=3760$ μm) is much larger than its width ($L_y=50$ μm). Therefore, the one-dimensional description used in the numerical simulations is justified for $t>L_y^2/D_{\rm ambi}\approx4$ ns [cf. Eq. (14)]. The diode has selective Ohmic contacts to the *n* layer (Ge/Au annealed at 425°C) and to the *p* layer (Zn/Au annealed at 425°) at both ends. This enables us to apply three independent voltages: $U_{pn}^{\rm l(eft)}$ (at $x=-L_x/2$), $U_{pn}^{\rm r(ight)}$ (at $x=+L_x/2$) and $U_{\rm lat}(=U_{nn})$ (see Fig. 2). However, as mentioned above, we choose $U_{pn}^{\rm l}=U_{pn}^{\rm r}=:U_{pn}$.

B. Pump-and-probe experiments

Our experiment is a pump-and-probe experiment based on the electroabsorption (Franz-Keldysh effect) in the intrinsic layer of the diode. The pump laser pulse ($\tau_{\rm pump}\approx10$ ns, $\lambda_{\rm pump}=790$ nm, spot diameter ≈40 μm) excites electron-hole pairs in the intrinsic layer. These carriers are separated by the builtin voltage $U_{\rm bi}$ and by the additional reverse bias voltage U_{pn}. Since the net charge within the layers is reduced by the photogenerated carriers, the original field in the intrinsic layer is partially screened. This enhances the transmission of the probe laser pulse ($\tau_{\rm probe}\approx1$ ns, $\lambda_{\rm probe}=900$ nm, spot diameter ≈40 μm), which follows the pump pulse with a variable delay *t*. This delay is adjusted by a double pulse generator. Repeating the pump-and-probe cycle at 100 kHz and chopping the pump laser at a frequency of 35 Hz, we can measure the transmission change caused by

the induced charge carriers at the probing spot x at delay time t using lock-in technique. The setup allows for both spatially and time-resolved transmission change measurements, including spatial coincidence. The experimental setup will be discussed in more detail in a subsequent paper.[10]

IV. RESULTS

The discussion of the obtained experimental results will be restricted to one set of parameters. We choose a reverse bias $U_{pn}=-6$ V and compare the two lateral voltages $U_{\mathrm{lat}}=0$ V and 20 V. Solving Poisson's equation for $\phi_n-\phi_p=-6$ V and taking into account a surface band bending of about 0.7 eV$\approx E_g/2$, we expect for the two-dimensional dark carrier concentrations $n_0=1.68\times10^{11}$ cm^{-2} and $p_0=3.1\times10^{12}$ cm^{-2}, respectively. Using the carrier mobilities obtained from Hall measurements, $\mu_n=5315$ cm^2/V s and $\mu_p=325$ cm^2/V s, and the capacity density of the diode at $U_{pn}=-6$ V, $C_{pn}\approx12$ nF/cm^2, we can calculate the ambipolar diffusion constant and the ambipolar mobility for the small-signal case:

$$D_{\mathrm{ambi}}(\rho=0)=D_{\mathrm{ambi}}^{\mathrm{bulk}}(\rho=0)+D_{\mathrm{ambi}}^{p\text{-}i\text{-}n}(\rho=0)$$
$$\approx 17\ \mathrm{cm^2/s}+6320\ \mathrm{cm^2/s}$$
$$\approx 6300\ \mathrm{cm^2/s}, \tag{14}$$

$$\mu_{\mathrm{ambi}}^{p\text{-}i\text{-}n}(\rho=0)\approx 2700\ \mathrm{cm^2/V\,s}. \tag{15}$$

In order to illustrate the experimental results, we first discuss the results expected from the numerical integration of Eq. (12), taking into account the boundary conditions given by the fixed values of the electric potential at the contacts. The pump laser pulse excites a total of $N\approx7\times10^7$ electron-hole pairs during the time between $t=-5$ ns and $t=+5$ ns at $x=0$ [center of the device, cf. Fig. 3(a)]. The excited carriers are assumed to be generated directly in the doping layers, whereas really the separation takes a few picoseconds. The calculated distributions of excess carriers for different times after excitation are depicted in Fig. 3(b). Let us first have a look at the calculated distributions without an externally applied electric field ($U_{\mathrm{lat}}=0$ V), i.e., at the ambipolar diffusion without drift (dash-dotted lines in Fig. 3). Due to the deviation from the small-signal case, the distribution deviates slightly from the Gaussian shape for small times ($t=25$ ns). When the carrier concentration decreases, the diffusion coefficient approaches the small-signal value and the resemblance of the distribution with the Gaussian shape predicted for the small-signal case by Eq. (13) increases. After 1000 ns, the approximate analytical solution again fails due to the finite size of the sample. The carriers recombine via the external circuit and the excess carrier concentration at the contacts vanishes due to the boundary condition $\phi_p-\phi_n=U_{pn}$.

With $U_{\mathrm{lat}}=20$ V (left, negative; right, positive), the distribution drifts towards the positive contact. This is just the same behavior as known from the ambipolar drift in bulk material, which is just the general case of minority carrier drift. The distribution of excess carriers moves to the drift direction of the *individual* minority carriers (electrons). Although the *individual* majority carriers drift into the opposite direction, the *excess concentration* shifts in the same direction as the minority carriers are drifting. This is because the minority carrier current increases due to the increased carrier concentration on the one hand. On the other hand, the external lateral field is screened by the additional carriers, which in turn decreases the majority carrier current. This is a result of the condition that no unscreened net charges may occur. In contrast to ambipolar drift in bulk semiconductors, our p-i-n structures offer the possibility to observe this process over a long time and over long distances.

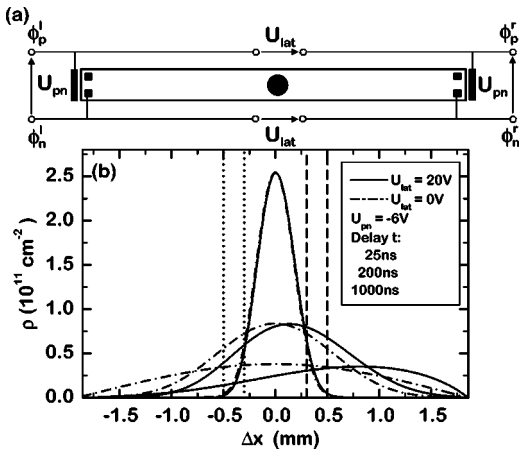

FIG. 3. (a) Illustration of the experimental setup and the applied voltages; the carriers are excited in the middle of the sample. (b) Calculated excess carrier concentrations 25 ns, 200 ns, and 1000 ns after the excitation for $U_{\mathrm{lat}}=0$ V (dash-dotted lines) and for $U_{\mathrm{lat}}=20$ V (solid lines).

In the experiment, we probe the carrier concentration at several different positions as a function of the time delay between pump and probe. For the sake of simplicity, we restrict the discussion to two distances from the excitation spot: $x_{1,1}=\pm300$ μm and $x_{2,2}=\pm500$ μm. These positions are indicated in Fig. 3(b). The excess carrier densities for negative x were not obtained by moving the probe position to the other side of the pump spot, but by changing the polarity of U_{lat}, which makes no difference since the pump spot is in the center of the sample.

Figure 4 depicts the measured time-resolved relative transmission changes due to the electro-absorption in the intrinsic layer of the diode with $U_{\mathrm{lat}}=0$ V (dotted lines) and $U_{\mathrm{lat}}=\pm20$ V (solid lines) at (a) $x_{1,1}=\pm300$ μm and (b) $x_{2,2}=\pm500$ μm.

In order to interpret the measured data, we need to know how the optical transmission change is linked to the excess carrier density. Therefore, we determined both the dependence of the carrier density on U_{pn} by conductivity measurements and the relation between transmission and U_{pn}. Thus, we can evaluate the time-resolved excess carrier concentrations from the measured transmission. These are shown in Fig. 5 for the two mentioned distances from the pump position. Theory and experiment agree well for $U_{\mathrm{lat}}=0$ and for positive x with $U_{\mathrm{lat}}>0$.

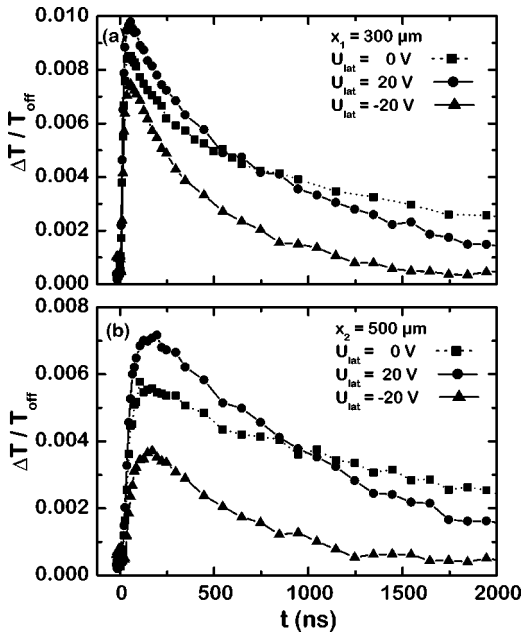

FIG. 4. The measured relative transmission change of the probe pulse due to the excess carriers over the time delay between pump and probe at (a) $x_1=300\ \mu$m and (b) $x_2=500\ \mu$m.

However, the measured carrier concentrations at negative x are significantly lower than those obtained from the simulation. This is possibly due to the holes generated in the zone between the center of the n channel and the surface. Due to the surface band bending these holes are driven towards the surface. Although the number of carriers generated in this region amounts to about 15% of the total number of carriers generated between the p layer and the center of the n channel

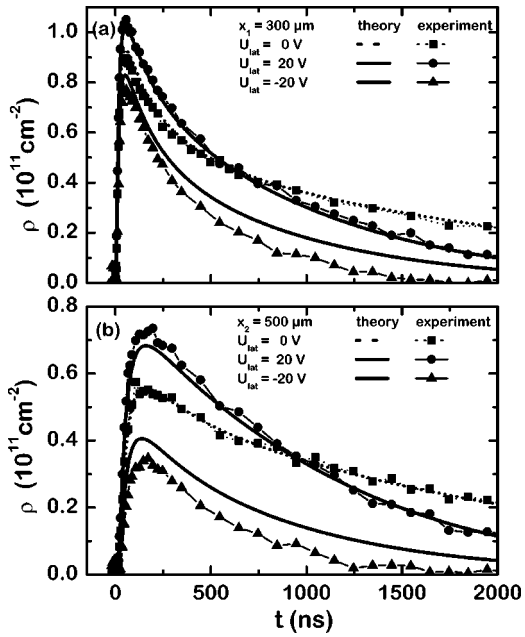

FIG. 5. The experimental and theoretical excess carrier concentrations over the time after excitation $U_{\rm lat}=0$ V, 20 V and -20 V at (a) $x_1=300\ \mu$m and (b) $x_2=500\ \mu$m.

(i.e., those expected to contribute to the ambipolar signal), they have been neglected in our simulations. This is justified in the case of zero lateral field. As these holes are trapped in surface states, they recombine locally with the corresponding electrons within the region of excitation. Therefore, they do not contribute to the transport. The situation changes if a negative lateral bias is applied. In this case, this hole charge (representing the minority species with regard to the electrons in the channel) is drifting in the negative x direction (with a low mobility and, hence, low drift velocity). Thus, the apparently too fast decrease of ρ at negative x could be an artifact of the surface hole drift: As the time between subsequent pulses is 10 μs in our experiments, the signal reflects the difference between the transmission at the delay time $0<t<2\ \mu$s and the transmission at $t\gg 10\ \mu$s. Thus, if, for instance, it takes somewhat less than 10 μs for the maximum of the drifting hole pulse to reach the observation point x, during the time $0<t<2\ \mu$s the surface charge at x is still determined by the decreasing contribution of the previous pulse, while the increase due to the ''new'' pulse will arrive there only at $t>2\ \mu$s. Thus, during the interval $0<t<2\ \mu$s the surface zone yields an increasing contribution to the absorption, as the reduced surface band bending, caused by the previous pulse, is recovering. Therefore, the transmission during this time is actually lower than expected from the theoretical simulations that neglect the surface contribution. It should be noted that the situation for positive x is not affected by this effect, for the same reasons as in the case without lateral bias.

From the data obtained by the numerical simulation we could extract time-dependent ambipolar mobilities and diffusion coefficients by evaluation of the mean position of the excess carriers and the time derivative of the mean variance of the excess carrier distribution respectively. The time evolution of the mean position of the excess carriers would yield a drift velocity and thus the ambipolar mobility, whereas the diffusion coefficient could be obtained by taking the time derivative of the mean variance of the excess carrier distribution. Or we could simply plot the coefficients used in the numerical simulation as a function of time and space.

However, we intend to extract estimates of the coefficients from the experiment, i.e., from the measured time evolution of the carrier densities at only a few individual probe positions. Different methods have been used to evaluate the ambipolar diffusion coefficient, e.g., from the time dependence of the carrier concentration or the current in one layer at one position.[7–9] All of these methods rely on the small signal solution of Eq. (12), i.e., Eq. (13). We propose a further method here, which also makes use of Eq. (13). If the excess carrier concentration is of the same order as the dark carrier concentration of the minority carriers, which is true in our experiment, the small-signal solution is no longer satisfactory, but we can still use a Gaussian function, however, with time-dependent parameters

$$\rho(x,t>0)=\frac{N}{\sqrt{4\pi t D^*_{\rm ambi}(t)}}\exp\left(-\frac{[x-v^*_{\rm drift}(t)t]^2}{4D^*_{\rm ambi}(t)t}\right), \tag{16}$$

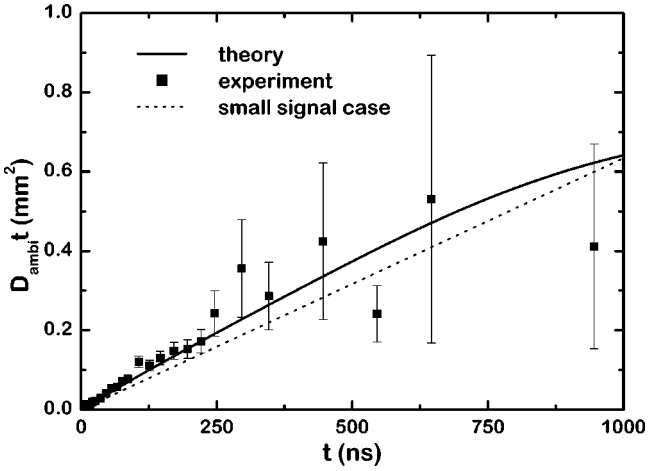

FIG. 6. Square of the ambipolar diffusion distance obtained by Eq. (17) from the experimental data (dots) and the numerical simulation (solid line). The small signal diffusion constant ($D_{\mathrm{ambi}} = 6337\ \mathrm{cm}^2/\mathrm{s}$) is indicated by the dotted line.

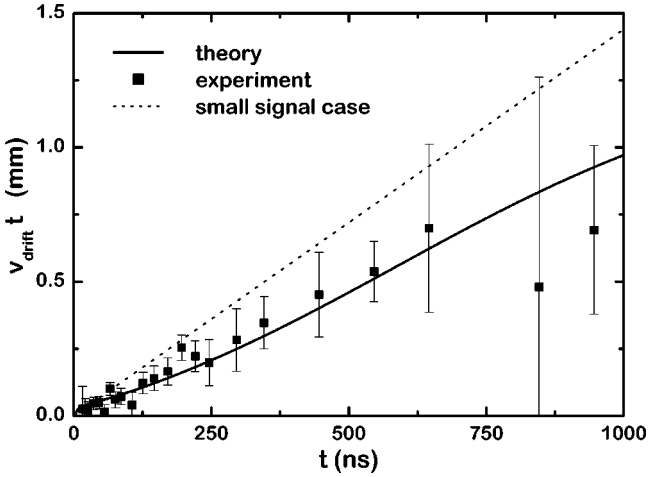

FIG. 7. Estimate of the ambipolar drift velocity obtained by Eq. (18) from the experimental data (dots) and the numerical simulation (solid line). The small-signal drift velocity ($v_{\mathrm{drift}} = 1440$ m/s) is indicated by the dotted line.

as a fit to the measured data. The parameters $D^*_{\mathrm{ambi}}(t)$ and $v^*_{\mathrm{drift}}(t)$ then provide an estimate for the diffusion and drift behavior of the excess carrier distribution. However, they are not the diffusion coefficient and the drift velocity, since the do not reflect the spatial dependence of these variables.

Since the origin of the deviations from the numerical simulation at negative x is not quite clear, we use the carrier concentrations at the two probe positions $x_1 = 300\ \mu$m and $x_2 = 500\ \mu$m to determine $D^*_{\mathrm{ambi}}(t)$ and $v^*_{\mathrm{drift}}(t)$. Let $\rho^0_{1,2}$ denote the excess carrier concentration for $U_{\mathrm{lat}} = 0$ V at x_1 and x_2, respectively, and $\rho^+_{1,2}$ the concentrations at the two positions for $U_{\mathrm{lat}} = 20$ V.

For zero applied lateral field, the drift velocity is obviously zero. Therefore Eq. (16) yields:

$$\ln\frac{\rho_1^0}{\rho_2^0} = \frac{x_2^2 - x_1^2}{4D^*_{\mathrm{ambi}}(t)t} \Rightarrow D^*_{\mathrm{ambi}}(t) = \frac{x_2^2 - x_1^2}{4t\ln(\rho_1^0/\rho_2^0)}. \qquad (17)$$

If we plot $D^*_{\mathrm{ambi}}(t)t$ vs t, in the small-signal case we would obtain a straight line through the origin whose slope is the diffusion constant. If however the small-signal condition does not hold, the diffusion coefficient is expected to exceed its small-signal value [cf. Eq. (12)]. In Fig. 6, we show the results obtained for $D^*_{\mathrm{ambi}}(t)t$ from the numerical simulation (solid line) and from our measured data (dots). The dotted line indicates the line expected in the small-signal case without boundary conditions [i.e., $L_x \to \infty$, cf. Eq. (13)]. The experimental values correspond very well with the theoretical curve, the slope of which ranges between 8000 cm^2/s immediately after the excitation and decreases towards its small-signal value after about 700 ns. The curve then becomes less steep than the small-signal line due to the carriers arriving at the contacts.

Similarly, one can obtain an estimate of the drift velocity of the excess carrier distribution from Eq. (16) as follows:

$$\frac{\ln(\rho_1^+/\rho_2^+)}{\ln(\rho_1^0/\rho_2^0)} = \frac{x_2^2 - x_1^2 - 2(x_2 - x_1)v^*_{\mathrm{drift}}(t)t}{x_2^2 - x_1^2}$$

$$\Rightarrow v^*_{\mathrm{drift}}(t) = \left(1 - \frac{\ln(\rho_1^+/\rho_2^+)}{\ln(\rho_1^0/\rho_2^0)}\right)\frac{x_2 + x_1}{2t}. \qquad (18)$$

The small-signal ambipolar mobility calculated in Eq. (13) corresponds to an ambipolar drift velocity of $v_{\mathrm{drift}} \approx 1440$ m/s. In Fig. 7, $v^*_{\mathrm{drift}}(t)t$, obtained according to Eq. (18) from the experimental and numerical data, is plotted versus t. The small-signal value is indicated by the dotted line. Again we observe the behavior we expect from Eq. (12): the drift velocity, i.e., the slope of the curve is always smaller than expected for the small-signal case, but approaches this value for times up to about 500 ns. The slope of the calculated curve ranges between $v^*_{\mathrm{drift}}(t = 150\ \mathrm{ns}) = 820$ m/s and $v^*_{\mathrm{drift}}(t = 800\ \mathrm{ns}) = 975$ m/s. Again, the deviation from the expected small signal behavior for times larger than 700 ns is due to the finite size of the sample. In an infinite sample, the slope would asymptotically approach the small signal line.

V. CONCLUSIONS

We have shown that the lateral transport of photogenerated charge carriers in the doping layers of a p-i-n diode can be described as a combined drift and diffusion. This process differs from bulk semiconductor ambipolar transport mainly with respect to the strongly enhanced diffusion process. Interestingly, the drift component in the case of equal lateral fields in both layers is essentially the same as that in bulk semiconductors. However, it can be observed much easier due to the extremely enhanced recombination lifetimes. Our spatially and time-resolved pump-and-probe experiments

have quantitatively confirmed the theoretical predictions. Finally we proposed methods for the determination of the ambipolar diffusion coefficient and the drift velocity.

In this paper we have investigated only the case that electrons and holes experience the same in-plane fields, although in Sec. II we have also derived the equations describing the general case of different in-plane fields $E_p^0 \neq E_n^0$. This case can be realized in *p-i-n* diodes and *n-i-p-i* structures (in contrast to bulk semiconductors) by a suitable choice of three different voltages (U_{pn}^{l}, U_{pn}^{r}, and U_{pp}, e.g.) applied to a structure with two Ohmic *n*- and two Ohmic *p*-layer contacts as depicted in Fig. 2. Without entering deeply into the details we want to outline how the ambipolar transport of photogenerated carriers may be affected in this scenario. First we note that in this case the steady state fields E_p^0 and E_n^0 will no longer be uniform within the sample even in the dark case. The spatial dependence of $E_p^0(x)$ and $E_n^0(x)$ follows from the condition of continuity for the electron and hole current densities together with the condition for the local electron and hole densities $p(x)-p^{\mathrm{th}}=n(x)$ as a function of the local difference $\phi_n(x)-\phi_p(x)$ of electric potentials for the electrons and holes. For the simple case of a δ-doped *p-i-n* diode with a threshold voltage U_{pn}^{th} for total electron depletion in the *n* layer and a residual hole density p^{th} this relation reads

$$p(x)-p^{\mathrm{th}}=n(x)=\frac{C_{pn}}{e}\{[\phi_n(x)-\phi_p(x)]-U_{pn}^{\mathrm{th}}\}. \quad (19)$$

For $p^{\mathrm{th}} \gg n(x)$ we obtain a nearly uniform field $E_p^0(x)=E_p^0=U_{pp}/L_x$. If the reverse voltages are chosen such that $|U_{pn}^{\mathrm{r}}|<|U_{pn}^{\mathrm{l}}|<|U_{pn}^{\mathrm{th}}|$, the electron density increases from left to right, whereas the magnitude of the field $E_n^0(x)$ decreases correspondingly, as the electron current density has to be independent of *x*. With the sign of $U_{pp}=U_{\mathrm{lat}}$ chosen as before, the pulse of photogenerated carriers will still move to the right contact with positive drift velocity as long as $|E_n^0(x)|>[n(x)/p(x)]|E_p^0|$ still holds [see drift term in Eq. (12)]. If, however, $|U_{pn}^{\mathrm{l}}|$ approaches $|U_{pn}^{\mathrm{th}}|$ there will be an increasing region where $|E_n^0(x)|<[n(x)/p(x)]|E_p^0|$ holds for any *x* larger than a critical x_{cr}. Under these circumstances the drift velocity of the pulse will have opposite sign if the illumination spot is located within the range $x_{\mathrm{cr}}<x<L_x$. In this case the excess carrier distribution will always drift towards the point x_{cr}, unless $|E_n^0(x)|<[n(x)/p(x)]|E_p^0|$ holds everywhere. In the latter case the photoinduced excess carrier distribution, i.e., both the excess minority and the excess majority carrier distribution will drift into the drift direction of the majority carriers. This finding is exactly opposite to the well-known pseudoparadox concerning the ambipolar drift in usual bulk semiconductors.[3] These peculiarities have still to be proven by future experiments.

*Electronic address: beck@physik.uni-erlangen.de

[1] K.H. Gulden, H. Lin, P. Kiesel, P. Riel, and G.H. Döhler, Phys. Rev. Lett. **66**, 373 (1991).

[2] G.H. Döhler, Phys. Status Solidi **52**, 79 (1972); **52**, 533 (1972).

[3] R. B. Adler, A. C. Smith, and R. L. Longini, *Introduction to Semiconductor Physics* (Wiley, New York, 1964).

[4] H. Schneider, E.C. Larkins, J.D. Ralston, J. Fleissner, G. Bender, and P. Koidl, Appl. Phys. Lett. **60**, 2648 (1992).

[5] G. Livescu, D.A.B. Miller, T. Sizer, D.J. Burrows, J.E. Cunningham, A.C. Gossard, and J.H. English, Appl. Phys. Lett. **54**, 748 (1989).

[6] P.J. Poole, C.C. Phillips, M. Henini, and O.H. Hughes, Semicond. Sci. Technol. **8**, 1750 (1993).

[7] G. Klem, P. Kiesel, A. Förster, and G. H. Döhler, in *Proceedings of the 23rd International Conference on the Physics of Semiconductors*, edited by M. Scheffler and R. Zimmermann (World Scientific, Singapore, 1996), p. 2299.

[8] D. Streb, G. Klem, W. Fix, P. Kiesel, and G.H. Döhler, Appl. Phys. Lett. **71**, 1501 (1997).

[9] D. Streb, M. Vitzethum, P. Kiesel, M. Kneissl, and G.H. Döhler, Superlattices Microstruct. **25**, 21 (1999).

[10] M. Vitzethum, D. Streb, M. Beck, P. Kiesel, S. Malzer, and G. H. Döhler (unpublished).